the second part of Eq. (19) can be written as vector equations with the definition of Eq. (12). Note that $\underset{\sim}{D}_1$ is zero and that we need to solve only two vector equations:

$$a\,\underset{\sim}{F}_2 = \underset{\sim}{D}_2, \qquad a\,\underset{\sim}{F}_3 = \underset{\sim}{D}_3 \tag{20}$$

2) With $\underset{\sim}{w}$ *and* F known from step 1, compute

$$A'_J = A_J - E^T F \tag{21}$$

and

$$\underset{\sim}{r}'_J = \underset{\sim}{r}_J - E^T \underset{\sim}{w} \tag{22}$$

and then solve

$$A'_J\,\underset{\sim}{\delta}_J = \underset{\sim}{r}'_J \tag{23}$$

which can be done easily since A'_J is a 3×3 matrix, and it is simple to solve a 3×3 system to obtain $\underset{\sim}{\delta}_J$.

3) Now compute

$$\underset{\sim}{\Delta} = \underset{\sim}{w} - F\,\underset{\sim}{\delta}_J \tag{24}$$

The above-described algorithm has been applied to problems where the Mechul function approach had been required previously. The results have shown it to be more convenient to use with considerable savings of computer time. It can be expected that these savings will be even greater for problems involving a larger number of differential equations.

Acknowledgments

This work was sponsored by the Air Force Office of Scientific Research under Contract AFOSR-900262.

References

[1]Bradshaw, P., Cebeci, T., and Whitelaw, J. H., *Engineering Calculation Methods for Turbulent Flows,* Academic, New York, 1981.

[2]Klineberg, J. M., and Steger, J. L., "On Laminar Boundary-Layer Separation," AIAA Paper 74-94, 1974.

[3]Keller, H. B., "The Bordering Algorithm and Path Following Near Singular Points of Higher Nullity," *SIAM Journal on Scientific and Statistical Computing,* Vol. 4, No. 4, 1983, pp. 573-582.

[4]Keller, H. B., "A New Difference Scheme for Parabolic Problems," *Numerical Solution of Partial-Differential Equations,* Vol. II, edited by J. Bramble, Academic, New York, 1970.

[5]Veldman, A. E. P., "New Quasi-Simultaneous Method to Calculate Interacting Boundary Layers," *AIAA Journal,* Vol. 19, 1981, p. 769.

[6]Carter, J. E., and Wornum, S. F., "Solutions for Incompressible Separated Boundary Layers Including Viscous-Inviscid Interaction," NASA SP-347, 1975.

Stratified Flow Around an Axisymmetric Body at Small Angle of Attack

H. E. Gilreath*

Johns Hopkins University, Laurel, Maryland 20723

Background

THE characterization of the internal wavefield produced by the wake of a vehicle moving in a stratified fluid is a problem in statistics. The recognition that the wavefield contains a prominent random component, generated by wake turbulence, led to the application of experimental methods based on ensemble averaging so that both the stochastic radiation and the mean properties of the wavefield could be described. For convenience of study, the mean properties can be thought to be built from a number of separate sources: body displacement, wake collapse (i.e., a sudden flattening of the wake by hydrostatic forces), propeller swirl, and hydrodynamic lift. In reality, all are coupled in a complicated manner, and shuffle in relative importance as operating conditions change.

The first published results from the ensemble testing program appeared in Ref. 1. These results not only confirmed the importance of the turbulence-generated random internal wavefield, but among other things, they revealed the existence of a sizable propeller-induced wavefield. This particular component was isolated by reducing the mean wavefield into even and odd parts (with respect to the axis of travel) and associating the antisymmetric part with propeller influences. Here we will be interested in the average symmetric wavefield only, so these influences must be removed. Nominally, all of the tests reported in Ref. 1 were conducted at zero angle of attack, and, in the present context, they serve as a baseline for studying the added effects of hydrodynamic lift.

When an axisymmetric body moves at an angle of attack, it generates lift even in the absence of wings or control surfaces. At large angle of attack (say $\alpha > 5$ deg), the resulting circulation can be considered to be deposited into the wake in the form of a turbulent vortex pair. This description is unlikely to be completely adequate at the small incidence angles of interest here—the vorticity being more distributed. However, regardless of the details, net vertical momentum is imparted to the wake, altering both its dynamic and kinematic development, and, in particular, its capacity to generate internal waves.

Existing analytical procedures for estimating the lift coefficient (C_L) of a streamlined, axisymmetric body as a function of its angle of attack cannot be criticized for being overly refined. At one extreme, slender body theory predicts the lift coefficient to be zero, which obviously is of no help in formulating a forcing mechanism for wave theory. The state of the subject is summarized in Ref. 2, where one is discouraged to find that estimates of C_L can differ by more than a factor of 2. This circumstance naturally presents difficulties in comparing theory and experiment, but we will see that choosing an intermediate value of C_L appears to produce reasonable results.

An approximate theoretical description of the kinematics of a turbulent mass with vertical momentum, rising in a stratified medium, has been given by Tulin and Shwartz[3] using similarity arguments. Although this theory is rudimentary and somewhat removed from the present flow situation, it has the virtue of being simple and, for this reason, was the first candidate examined.

Results and Discussion

Internal Wave Experiments

The experiments were conducted in the 30-ft towing basin at the Applied Physics Laboratory Hydrodynamics Research Laboratory. The testing procedure are described fully in Ref. 1, where it is noted that extraordinary care was needed to assure that the test conditions were very nearly identical for each member of the ensemble. Measurements in the (deterministic) potential flow region indicated that the standard error in vertical displacement was only 0.1% of the vehicle diameter. For the present tests, the single-electrode conductivity probes, used for measuring vertical displacements, were arranged as shown in Fig. 1. This figure also defines the coordinate system.

The test vehicle (12:1 fineness ratio) was operated at an average angle of attack of -2.0 deg (nose down). The present ensemble consisted of 20 individual runs at an internal Froude number (F) of 52, where $F = 2\pi V/ND$ and $N^2 = -g/\rho(\mathrm{d}\rho/\mathrm{d}z)$ (N is the Brunt-Vaisala frequency). The ensemble-averaged

Received May 21, 1990; revision received Oct. 17, 1990; accepted for publication Oct. 23, 1990.

*Principal Staff Engineer, Milton S. Eisenhower Research Center, Applied Physics Laboratory.

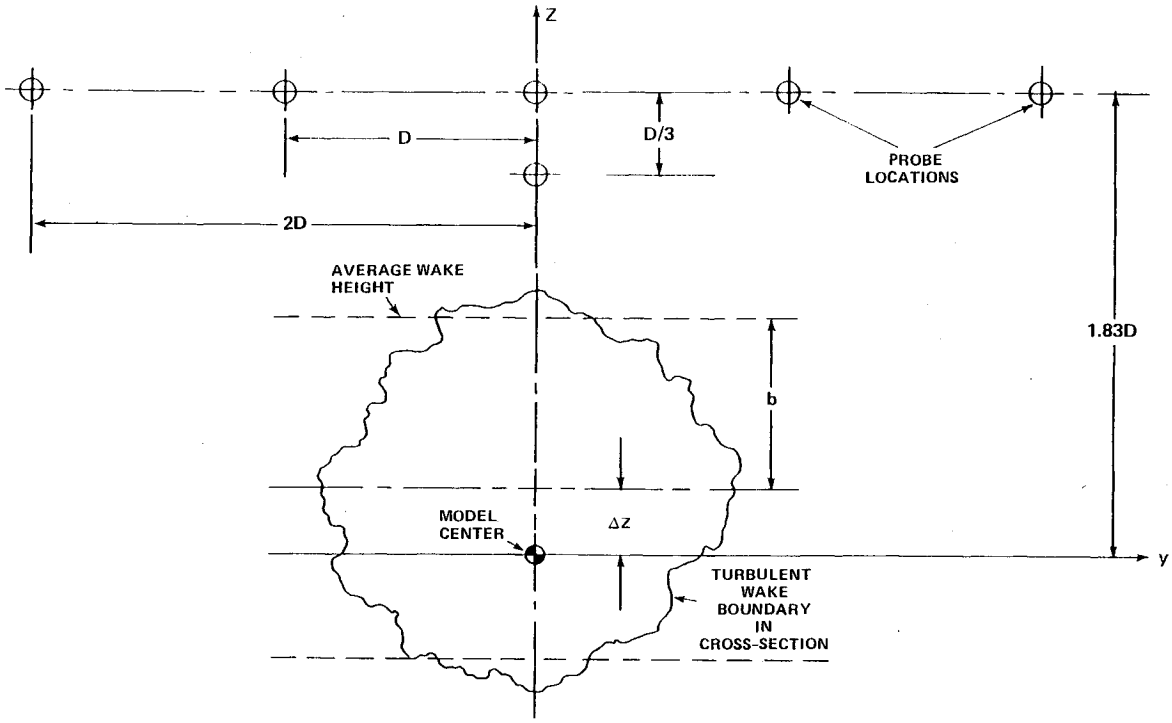

Fig. 1 Probe array configuration and definition of wake variables.

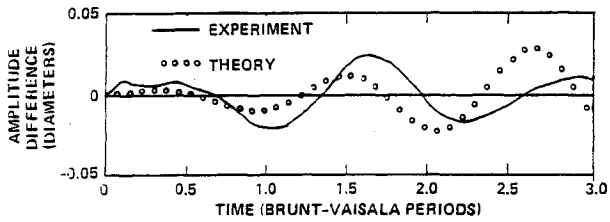

Fig. 2 Comparison of difference waveform to theory at $y/D = 1.0$.

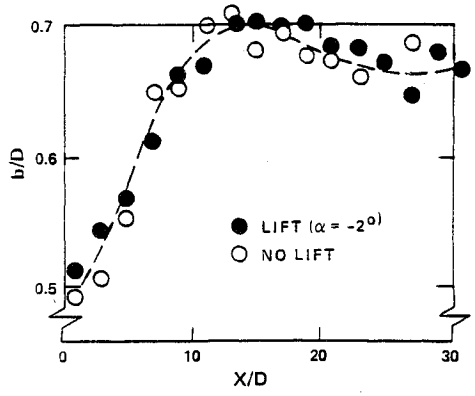

Fig. 3 Comparison of ensemble-averaged wake heights with and without lift.

vertical displacement records were reduced into even and odd parts according to

$$\delta = \tfrac{1}{2}[\delta(y) \pm \delta(-y)]$$

where addition is associated with the even component and subtraction with the odd component.

At small angles of attack, the total vertical force coefficient for an axisymmetric body can be estimated by[2]

$$C_V = [C_D + 8\kappa(\delta_l^*/D)^2]_{\alpha=0}\,\alpha + [(4/\pi)\eta\phi\bar{C}_{DC}]\alpha^2$$

where

C_D = body drag coefficient, based on cross-sectional area
κ ≡ ratio of effective base area to wake displacement area
δ_l^* ≡ displacement thickness of boundary layer at body tail
l = body length
α = angle of attack
D ≡ maximum body diameter
η ≡ body shape factor, $= 2\int_0^1 (r/D)d(x/l)$
ϕ ≡ fineness ratio, l/D
$\bar{C}_{DC}$ ≡ crossflow drag coefficient, based on maximum body diameter

When defensible estimates are made for the empirical parameters, κ and $\bar{C}_{DC}$, the force coefficient for $\alpha = -2$ deg varies between 0.036 and 0.085; but the values that seem in best agreement with the preponderance of existing data lead to $C_V = 0.057$, which is near the median of the range. In the work reported here, this number was used to compute the strength of the vertical force distribution used in the linear theory for the wavefield, assuming a "horseshoe" vortex configuration. An outline of the general theory is given in Ref. 1.

Since one expects the lift contribution to be symmetric with respect to the axis of travel, an estimate of this contribution can be obtained by forming the difference between the even parts of wave records obtained with and without lift at the same Froude number. Presumably, the remainder is free of contributions from body displacement and from the portion of mean wake-generated waves not associated with lift (cf. Ref. 1). Figure 2 shows the results of this subtraction procedure for probes located one body diameter off track. The lowermost solid line is the experimental difference waveform, and the circles symbolize the theoretical prediction obtained using linear theory. Note the reasonably good correspondence in maximum amplitude but little resemblance in spatial pattern.

Turbulent Wake Experiments

Figure 1 serves to define the geometrical variables used in studying the average evolution of the turbulent wake. The experimental data given in Fig. 3 were obtained by computing ensemble averages of digitized shadowgraph records. Note

that, when defined according to Fig. 1, the maximum wake radius, as well as the extent of wake collapse, is little affected by the presence of lift.

The wake centerline reaches its maximum excursion prior to the point of collapse. This result can be shown in an interesting way by plotting the wake half-height (b) as a function of the centerline deflection (Δz), as illustrated in Fig. 4. For self-similar flow in homogeneous surroundings, this plot would take the form of a straight line, with the slope being the so-called entrainment coefficient (β).

Space limitations do not permit a full discussion here of the Tulin-Shwartz similarity theory for turbulent vortex pairs.[3] It must suffice to point out that, if one chooses to ignore dissipation and asserts that the initial net buoyancy of the turbulent mass is zero, the problem reduces to an ordinary differential equation whose solution can be constructed formally from elliptic functions. This equation can be simplified even further

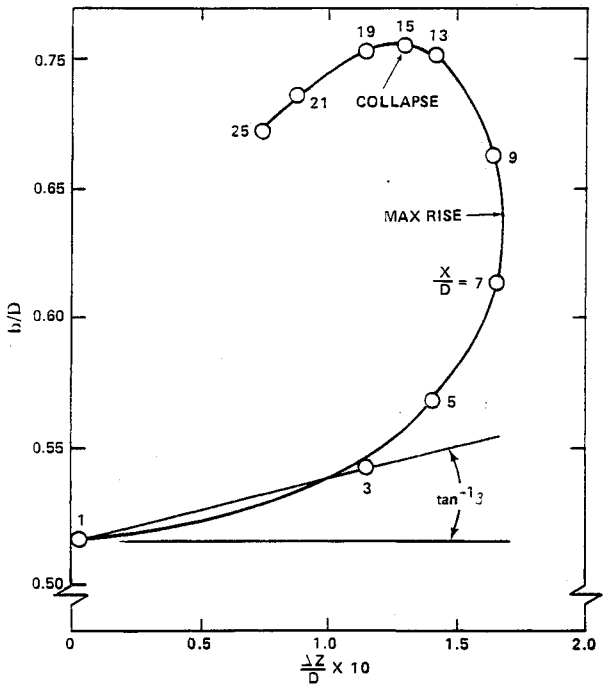

Fig. 4 Wake height vs centerline deflection.

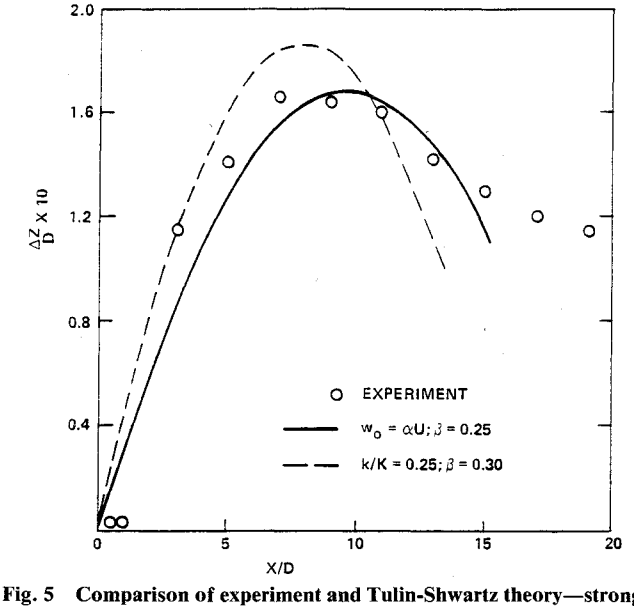

Fig. 5 Comparison of experiment and Tulin-Shwartz theory—strong stratification limit.

for cases in which buoyancy forces dominate (the situation of interest at early wake ages), which leads to

$$\frac{d\eta}{d\bar{t}} = (1 - 3B\eta)^{1/2}$$

where

η = $(z/z_0) - 1$
$\bar{t}$ = $w_0 t/z_0$
w_0 = vertical velocity at $t = 0$
z = location of wake centerline with respect to a virtual origin
z_0 ≡ $z@t = 0$
B ≡ $(2k/3k)(z_0 N/w_0)$
k = coefficient of virtual potential energy
K = coefficient of virtual kinetic energy

The solution of this equation is

$$\eta = \bar{t} - \frac{3B}{2}\left(\frac{\bar{t}^2}{2}\right)$$

so the turbulent mass behaves as a "particle" subject to the acceleration ($-3B/2$). This simple result predicts that

$$(\eta/\bar{t})_{\eta = \eta_{max}} = 0.5$$

From the experimental results, we estimate that

$$(\eta/\bar{t})_{\eta = \eta_{max}} = 0.55$$

Figure 5 compares two solutions for the centerline trajectory to experimental results. Given an experimental determination of the wake radius and initial vertical velocity, two empirical parameters are required for these solutions, β and k/K. We can expect the values of these parameters to vary from one class of flow to another, but if one blindly applies the values for these two parameters reported in Ref. 3, the dashed curve results, leading to a reasonable prediction of the maximum centerline excursion. Conversely, we can use the experimental data to determine k/K by requiring the maximum excursion to be matched. One solution of this type (denoted by the solid line in Fig. 5) leads to the estimate $k/K \doteq 0.12$, as contrasted to the value 0.25 reported for the vortex pairs studied in Ref. 3. This result implies a higher kinetic energy content in the case under study here.

In the absence of some generality in the empiricism, the application of the Tulin-Shwartz theory amounts to an exercise in curve fitting, and the room for improvement is obviously large; however, the theory at least provides a means for making simple estimates of the early wake trajectory, armed only with a rough idea of the magnitudes of the parameters involved.

Summary and Conclusions

Available analytical methods do not permit the lift coefficient (C_L) of an axisymmetric body to be established within a factor of about 2.5. The present results, however, indicate that using the median value for C_L, together with a simple horseshoe vortex lift model, yields a surprisingly good prediction of the maximum amplitude of lift-generated internal waves when linear propagation theory is applied. Although, at first appearance, the amplitude is predicted adequately, the spatial patterns of the theoretical and experimental wave records are considerably different, which perhaps indicates that the modeling of the spatial distribution of the lift force needs to be improved.

When plotted with respect to its own centerline, the vertical geometry of a stratified turbulent wake does not appear to be affected strongly by lift. The maximum wake height and extent of collapse are nearly the same for lifting and non-lifting

cases. This finding may suggest that, at small angles of attack, lift and wake-collapse sources of internal wave generation might be usefully considered as uncoupled.

The early trajectory of the wake centerline is fairly well predicted by the self-similar theory of Tulin and Shwartz, using reasonable values for the empirical parameters involved. The maximum excursion occurs prior to the onset of collapse.

Acknowledgments

The work was supported by the U.S. Navy Space and Naval Warfare Systems Command under Contract N00039-89-C-5301. The formulation of the linear solution for the propagation of lift-generated internal waves used here was first carried out by J. J. Riley, D. R. S. Ko, and R. E. Robins at Flow Research Company, Kent, Washington. The efforts of C. L. Yates, C. R. Walton, A. Brandt, and G. Dailey in helping to conduct the experiments and analyze the experimental data are much appreciated.

References

[1]Gilreath, H. E., and Brandt, A., "Experiments on the Generation of Internal Waves in a Stratified Fluid," *AIAA Journal,* Vol. 21, No. 5, 1985, pp. 693–700.

[2]Thwaites, B., *Incompressible Aerodynamics,* Oxford Press, London, 1960.

[3]Tulin, M. B., and Shwartz, J., "The Motion of Turbulent Vortex Pairs in Homogeneous and Stratified Media," Hydronautics, Inc., Tech. Rept. 231-13, Laurel, MD, April 1971.

Surface Grid Generation Based on Unstructured Grids

Masahiro Suzuki*
Institute of Computational Fluid Dynamics, Tokyo, Japan

Introduction

IT has been well recognized that the generation of surface grids for complex configurations requires a great deal of human labor, although the computational expense of setting up surface grids may not be prohibitive. Naturally, effective generation of surface grids has been the subject of considerable attention in the literature. The general methods to produce the grids for three-dimensional flowfields are numerous; however, the present capabilities of generating the surface grids are limited in scope and versatility. At this time, the generation techniques for surface grids are of two general types: 1) numerical solution of partial differential equations (PDE) and 2) algebraic interpolation. In general, both systems treat generating the surface grid as a two-dimensional boundary-value problem on a curved surface, which is specified by a quadrangular patch through the use of surface parametric coordinates. The generation of the surface grid is accomplished over several stages. First, the Cartesian coordinate values $r_{i,j}$ of the boundary points on the four edges of the surface grid are specified, converting these values to the surface parametric coordinate values $(u_{i,j}, v_{i,j})$ on the edges. Then, the interior values in the array $u_{i,j}$ and $v_{i,j}$ from the edge values are determined by interpolation or PDE solution. Finally, these parametric coordinate values are converted to the Cartesian coordinates $r_{i,j}$. This procedure requires a well-structured surface for the input data. In view of this stringent requirement, conventional surface grid generation is inefficient and laborious. In practice, the preparation of a large amount of input data is an extremely time-consuming task. The geometry data for complex configurations, which are often utilized in engineering applications, are customarily produced by use of a computer-aided design (CAD) system. Under idealized conditions, accurate input data for the surface definition would be available directly from the CAD package. However, in reality, the currently existing CAD software programs are, by and large, incapable of providing this vital information. At the present level of development, a series of cross sections, i.e., the one-dimensional arrays of x, y, and z coordinates, are usually extracted from the CAD package. It is important to note that these data are primitive or raw. The points sets or distributions vary widely among cross sections. The conventional surface grid generator needs a quadrangular patch for the input data of the geometry definition as mentioned earlier; these primitive data must be grouped into quadrangular patches, which constitute the basis for a global patch. For this purpose, several data processors, which use some forms of interpolation, have been developed.[1,2] However, it is difficult to connect the local patches and to lap a quadrangular patch around the computationally complex geometry. This geometry does not necessarily represent a whole body, but it denotes a surface in which one coordinate is kept constant. If the local patches cannot be connected into a global patch, the grids are generated on each local patch, and then these grids can be combined. Therefore, to ensure continuity of the slope and curvature between each block, special treatments are essential.

It is easier and more flexible to describe a complicated geometry by plural polygonal surface patches (referred to as the unstructured grid) rather than by a quadrangular patch. Consequently, it would be highly advantageous if a way could be found in which the unstructured grid could be utilized directly for surface grid generation. From this point of view, investigations have been pursued to devise a scheme based on the unstructured grid. In the present study, the basic idea of constructing the surface grid is similar to the two-dimensional grid generation technique of Rao et al.[3] They proposed a methodology using Laplace's equations, which are solved in the physical domain using the finite element technique. The curvilinear coordinate lines are constructed by utilizing the interpolation functions applicable within each element, and the grid inside the solution domain is produced. Thus, in contrast to the well-known elliptic grid generation equations solved in the computational domain,[4] the method of Ref. 3 avoids the need to solve nonlinear equations, and the orthogonality is satisfied. The implementation of the Dirichlet or Neumann boundary conditions, which relate to the grid spacing and the slope of grid lines at the boundary, is straightforward. Reference 3 employed the quadrangular element, and no efforts were made to create the structured grid from the unstructured grid. Rao et al. point out only the advantage of solving the Laplace equations in the physical domain. In the present work, the unstructured grid is introduced to solve Laplace's equations. This unstructured grid specifies the three-dimensional surfaces. The curvilinear coordinate lines are drawn by searching for the contours inside the solution domain, i.e., the three-dimensional surfaces, to produce the surface grids. By introducing the weighting function, as asserted by Thompson et al.,[4] the grid space control is also achieved.

Model

Finite Element Solution Procedure

The following PDEs are mapped and solved by a finite element method on the unstructured grid:

$$\nabla(\lambda \nabla \xi) = 0 \tag{1}$$

$$\nabla(\lambda \nabla \eta) = 0 \tag{2}$$

Received July 5, 1990; revision received Nov. 6, 1990; accepted for publication Nov. 9, 1990.

*Research Staff, 1-16-5 Haramachi, Meguro-ku, 152. Member AIAA.